Journal of Iron and Steel Research, International 24 (2017) 1109—1114

Contents lists available at ScienceDirect

Journal of Iron and Steel Research, International

journal homepage: www.chinamet.cn

In-situ microstructural evolutions of 5Mn steel at elevated temperature in a transmission electron microscope

Han-bo Jiang[1], Xi-nan Luo[1], Xiao-yan Zhong[1,*], Hui-hua Zhou[1], Cun-yu Wang[2], Jie Shi[2], Han Dong[2]

[1] National Center for Electron Microscopy in Beijing, Key Laboratory of Advanced Materials (MOE), State Key Laboratory of New Ceramics and Fine Processing, School of Materials Science and Engineering, Tsinghua University, Beijing 100084, China

[2] Central Iron and Steel Research Institute, Beijing 100081, China

ARTICLE INFO

Key words:
5Mn steel
Focused ion beam milling
In-situ observation
Microstructural evolution
Austenite
Cementite

ABSTRACT

The microstructural evolutions of 5Mn steel during various heat treatments have been investigated by in-situ transmission electron microscopy (TEM). The specimen of 5Mn steel was prepared using focused ion beam (FIB) milling, which allowed the selection of specific morphology of interest prior to the in-situ observation. The complete austenization at 800 ℃ was verified at the atomic scale by minimizing thermal expansion and sample drift in a heating holder based on micro-electro-mechanical-systems. During annealing at 650 ℃, the formation of reverted austenite was dynamically observed, while the morphologies of austenite laths of 5Mn steel after in-situ heating were quite similar to that after ex-situ intercritical annealing. During annealing at 500 ℃, the morphological evolution of cementite and associated Mn diffusion were investigated. It was demonstrated that a combination of FIB sampling and high temperature in-situ TEM enables us to probe the morphological evolution and elemental diffusion of specific areas of interest in steel at high spatial resolution.

1. Introduction

Recently, the 0.2 mass% C-5 mass% Mn steels (5Mn steel) have drawn a lot of attentions due to their extraordinary mechanical properties and potential applications in automobile industry[1,2]. In order to understand the structure-property relationship of 5Mn steels, the microstructural evolution and elemental diffusion under different heat treatment procedures have been carried out[3-13]. Moor et al.[3] and Lee et al.[4] reported that Mn partitioning was a key factor in stabilizing a high volume fraction of retained austenite in such steels at room temperature (RT), which improved the mechanical properties of 5Mn steels. Mn diffusion between austenite and ferrite during intercritical annealing[5-8], as well as the precipitation and coarsening behaviors of cementite[9-12], has also been investigated. Nonetheless, in most of the previous studies, ex-situ methods were applied to examine the microstructural evolution of 5Mn steels. Ex-situ experiments cannot dynamically track the phase transformation and elemental diffusion in the 5Mn steel during heat treatments. It is not possible to choose an area of interest containing specific microstructural features like grain boundaries, packet interfaces, lath interfaces, precipitates and see how a specific microstructure evolves at elevated temperature.

In-situ heating experiments in a transmission electron microscope (TEM) allow real-time observations of heat treatments of steels, including grain growth[14], recrystallization[15], dislocation propagation[16] and elemental diffusion[17]. Instead of performing heat treatments outside the microscope and then observing the samples post-mortem, in-situ microscopy allows direct observations of the dynamic behavior of steels under a variety of annealing conditions. In traditional in-situ heating TEM experiments, the spatial resolution was dramatically suppressed due to the sample drift induced by thermal expansion when an entire 3 mm-diameter TEM specimen was heated. Recently, the state-of-the-art in-situ TEM has been developed to study the microstructures at the atomic scale by using micro-electro-mechanical systems (MEMS)-based heating stages[18-20], which generally requires specimen prepared by focused ion

* Corresponding author. Assoc. Prof., Ph.D.
E-mail address: *xyzhong@mail.tsinghua.edu.cn* (*X.Y. Zhong*).

Received 23 January 2017; Received in revised form 20 March 2017; Accepted 22 March 2017
Available online 15 November 2017

beam (FIB) milling[21-23]. However, the traditional lift-out lamella prepared by FIB cannot precisely choose the area of interest, since the lamella was buried in the bulk materials before lifting out.

In this paper, FIB was used to cut out the specific area of interest from a regular 3 mm-diameter TEM sample of 5Mn steel after observing its microstructure in a TEM. Various in-situ observations were carried out on 5Mn steel during different heat treatment procedures in order to understand the phase transformation of 5Mn steel at different temperatures. Benefiting from an advanced MEMS-based heating system, the microstructural evolution in 5Mn steel can be observed at the atomic scale with minimum sample drift, while in-situ elemental diffusion can also be detected. In the example of 5Mn steel, it was demonstrated that the in-situ heating TEM experiments are increasingly able to provide fundamental information for understanding the microstructural evolution at the atomic scale and the elemental diffusion during the phase transformation.

2. Experimental Procedure

The steel with a chemical composition of 0.2 mass% C-5 mass% Mn was investigated. The sample was first prepared under vacuum using an induction furnace, then homogenized at 1250 ℃ for 2 h before forged into rods with diameter of 16 mm. Next, after austenization at 1200 ℃ for 30 min, the forged rods were water quenched to form complete martensite microstructure.

In order to prepare the in-situ TEM specimen with the specific area of interest, a conventional TEM specimen with 3 mm in diameter was first prepared. The sample was mechanically ground to 50 μm in thickness, then the sample foils were twin-jet polished in a solution of 7 vol. % perchloric acid and 93 vol. % alcohol at －20 ℃. After locating the area of interest in a TEM, the in-situ TEM specimen using Zeiss Auriga FIB was prepared. For example, Fig. 1(a) shows the microstructure and the selected area electron diffraction (SAED) patterns of the area of interest in an as-quenched sample, including martensite laths and packet interfaces without any cementite and retained austenite. As shown in the low-magnification TEM image in Fig. 1(b), the area of interest was marked by the white circle. In order to position the area of interest, the holes formed during twin jet thinning and the edge morphology of the TEM specimen were selected as the markers and indicated by the white arrows. As is shown in the scanning electron microscope (SEM) image of the corresponding sample in Fig. 1(c), the area of interest was also marked by the white circle and positioned by the corresponding markers as indicated by the white arrows. Here the relatively thick area was selected for in-situ experiments, since the microstructural evolution in the bulk materials during heat treatments takes place in the relatively large volume. Using FIB milling, the lamella with the size of 25 μm × 10 μm including the area of interest was lifted out and transferred onto the chips of DENS solutions in-situ heating holder. The MEMS-based holder provided an elevated temperature environment without reducing the resolution of a TEM. During in-situ heating TEM experiments, the microstructural evolutions and elemental mapping of 5Mn steel were carried out in FEI cubed Titan 80－300 with an image corrector, FEI Titan G²80-200 ChemiSTEM equipped with a probe corrector and the SuperX energy dispersive spectrometry (EDS) system with the four Bruker Silicon Drift Detectors,

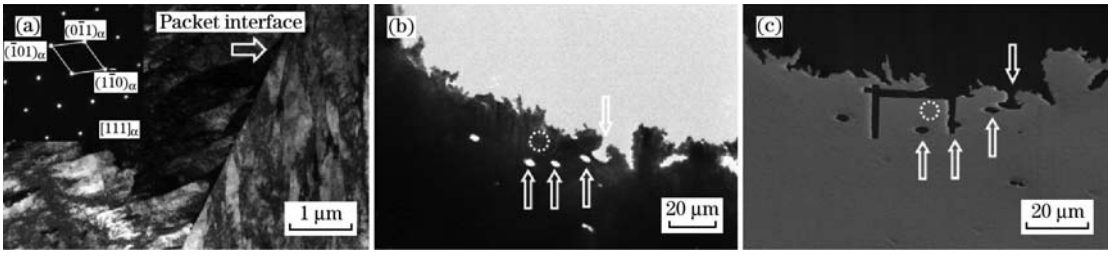

(a) Bright-field transmission electron microscope images and a selected area electron diffraction pattern from an area of interests including packet interfaces and lath interfaces; (b) Low-magnification TEM images of the interested areas; (c) Scanning electron microscopy images of corresponding interested area cut by focused ion beam milling.

Fig. 1. Locating interested areas of as-quenched 5Mn steel using TEM and FIB milling.

and FEI G²20.

3. Results and Discussion

In order to better understand phase transformation of 5Mn steel at different temperatures and determine the typical temperature for various heat treatments, the phase diagram of 5Mn steel was calculated using Thermo-Calc software, as shown in Fig. 2. Based on the calculated phase diagram, in-situ heat treatments at three annealing temperatures were carried out as marked by three stars in Fig. 2. Firstly, when the annealing temperature was set to

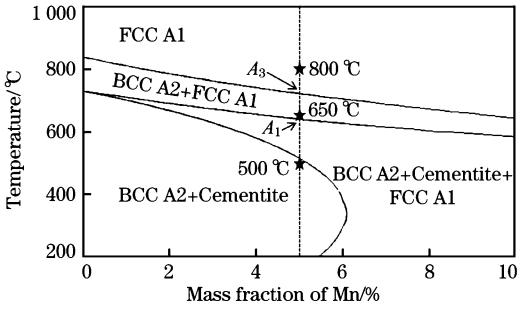

Fig. 2. Phase diagram of 5Mn steel calculated by Thermo-Calc software.

800 ℃ well above A_3 temperature, the complete austenization process was observed at the atomic scale. Secondly, when the annealing temperature was set to 650 ℃ between A_1 and A_3 temperatures, the nucleation and growth of austenite at matrix lath boundaries were studied. Thirdly, when the annealing temperature was set to 500 ℃ well below A_1 temperature, the formation and coarsening of cementite were focused on. All the annealing time at different temperatures was set to 40 min.

3.1. Complete austenization at 800 ℃

The as-quenched specimen was heated to 800 ℃ above the critical temperature A_3 of 723 ℃. All the martensite phases in as-quenched 5Mn steel were transformed to austenite phase. Fig. 3(a) shows the high resolution transmission electron microscopy (HRTEM) image of martensite phase at the atomic scale at RT before heating. Fig. 3(b) shows the HRTEM image of austenite phase at the atomic scale at 800 ℃ after complete austenization. The corresponding fast Fourier transformation (FFT) patterns shown in the insets of Fig. 3 clearly demonstrate the phase transition from martensite to austenite during in-situ HRTEM experiments following the Kurdjumov-Sachs (K-S) orientation relationship with $[111]_\alpha // [011]_\gamma$ and $(1\bar{1}0)_\alpha // (1\bar{1}1)_\gamma$.

The in-situ observation of complete austenization of 5Mn steel has been achieved at the atomic scale, benefiting from the minimized thermal expansion and specimen drift due to the high stability of the MEMS-based heating system. The temperature environment of the chip was locally controlled via a four-point-probe, which guaranteed the stability and accuracy (0.001 ℃ at any elevated temperature) during the course of heating in the experiment. Furthermore, the MEMS chip scaled down the heater to the micrometer size and had a very low thermal expansion coefficient, so sample drift was merely 0.5 nm per minute. The advantage of the MEMS-based heating system enables us to observe the in-situ experiment of complete austenization at the atomic level.

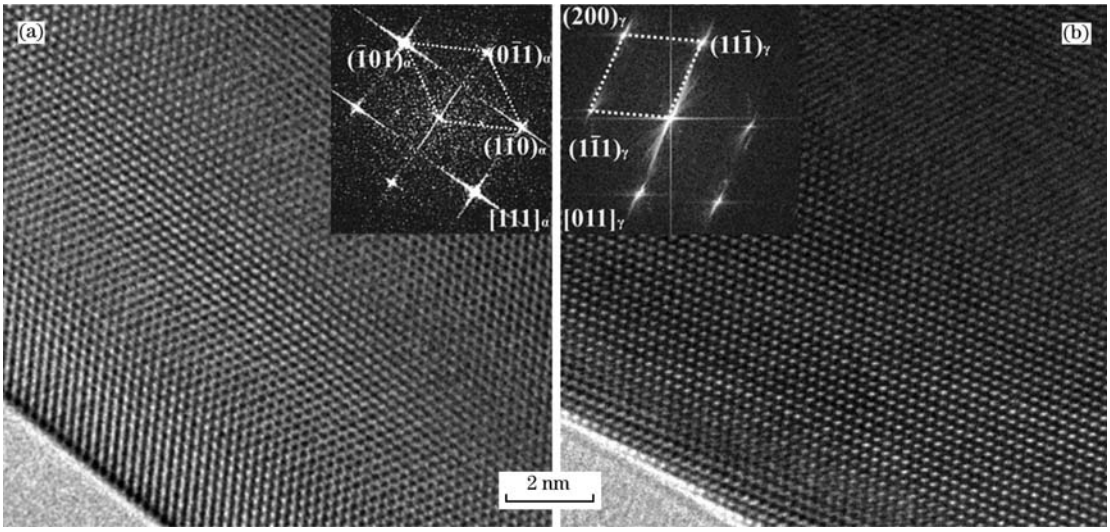

(a) Specimen at room temperature before heating; (b) Specimen at 800 ℃ after complete austenization.
The corresponding fast Fourier transformation patterns show that the phase transformation follows Kurdjumov-Sachs orientation relationship with $[111]_\alpha // [011]_\gamma$ and $(1\bar{1}0)_\alpha // (1\bar{1}1)_\gamma$.

Fig. 3. In-situ observation of complete austenization in 5Mn steel at 800 ℃ using high resolution transmission electron microscopy.

3.2. Nucleation and growth of austenite at 650 ℃

The as-quenched specimen was heated to 650 ℃ between the critical temperature A_1 of 643 ℃ and the critical temperature A_3 of 723 ℃. During the intercritical annealing, the in-situ nucleation and growth of reverted austenite has been observed. Fig. 4 shows the microstructural evolution at 7, 257, 548, 960, 1557, and 2356 s during the annealing procedure.

The solid arrows pointed out the nucleation and growth of the austenite located at matrix lath boundaries. The corresponding SAED pattern shown in the inset in Fig. 4(f) was indexed as austenite phase oriented along [112] zone axis. Based on the experimental observation, it was verified that the nucleation and growth of austenite particles preferred to take place at matrix lath boundaries, which was in agreement with the authors' previous studies of 5Mn steel after ex-situ intercritical annealing[8].

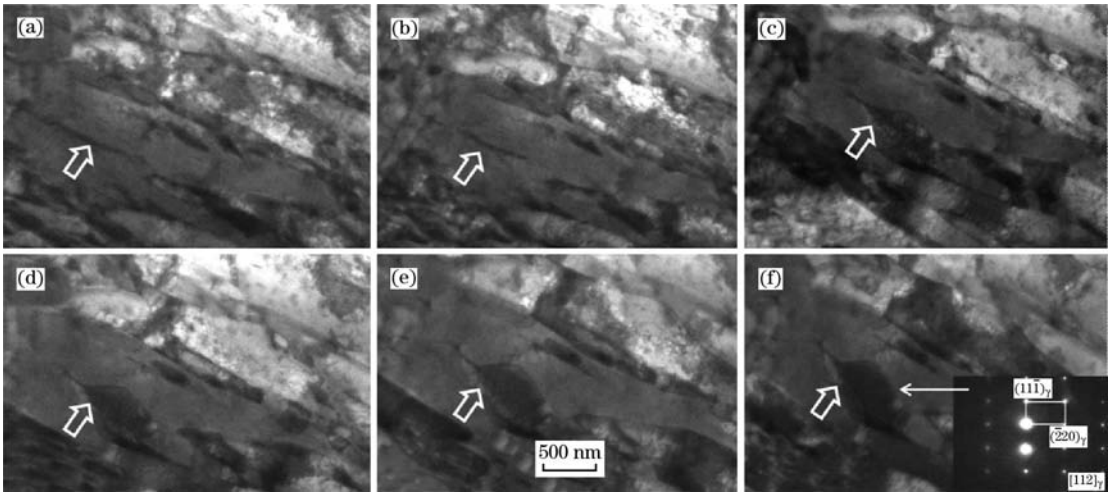

(a) Specimen annealed for 7 s; (b) Specimen annealed for 257 s; (c) Specimen annealed for 548 s; (d) Specimen annealed for 960 s; (e) Specimen annealed for 1557 s; (f) Specimen annealed for 2356 s. The selected area electron diffraction patterns show austenite phase along [112] zone axis indicated by the white arrow.

Fig. 4. In-situ observation of austenite nucleation and growth in 5Mn steel during annealing at 650 ℃.

After the in-situ heating experiments, the morphology and diffraction patterns of reverted austenite were investigated. Fig. 5(a) shows the about 60 nm wide austenite with twin structure. The corresponding SAED patterns of twin structure are shown in the inset of Fig. 5(a). The similar austenite with twin structure was also observed in 5Mn steel after ex-situ intercritical annealing, which might enhance mechanic properties during plastic deformation. The bright field and dark field TEM images, as shown in Figs. 5(b) and 5(c), respectively, reveal the austenite laths at matrix lath boundaries. The austenite in Fig. 5(b) followed the K-S orientation relationship with $[111]_\alpha // [011]_\gamma$ and $(1\bar{1}0)_\alpha // (1\bar{1}1)_\gamma$, which was clearly shown by SAED patterns in the inset of Fig. 5(b). The morphology of austenite was quite similar to the one observed in the 5Mn steel after ex-situ intercritical annealing in the previous work[8], indicating that evolution of austenite morphology during in-situ experiments was comparable with that

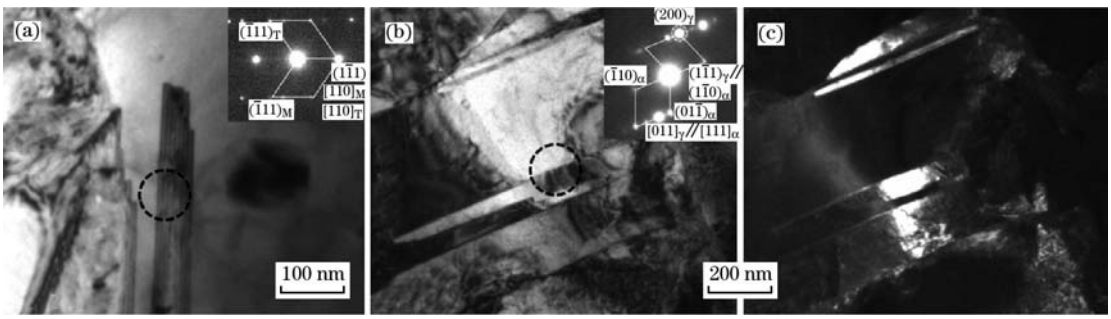

(a) Austenite laths with twin structure and corresponding selected area electron diffraction patterns taken from the area within black circle; (b) Austenite laths at matrix lath boundaries and the corresponding selected area electron diffraction patterns showing Kurdjumov-Sachs orientation relationship; (c) Corresponding dark field image of austenite laths by selecting (200) diffraction spot of austenite, marked by the white circle in the inset of (b).

Fig. 5. Fine structures of reverted austenite after in-situ annealing at 650 ℃.

during ex-situ experiments.

3.3. Coarsening of cementite precipitates at 500 ℃

The as-quenched specimen was heated to 500 ℃ well below the critical temperature A_1 of 643 ℃. The rate of heating from RT to 500 ℃ was 10 ℃/min. The microstructure and Mn distribution around martensite lath interfaces in as-quenched 5Mn steel

are clearly shown in Figs. 6(a) and 6(b), respectively. There was no significant segregation of Mn at lath interfaces as indicated by the dotted arrows. The Mn distribution of the as-quenched sample was relatively uniform. Figs. 6(c), 6(e) and 6(g) show the microstructural evolution at 0, 12 and 40 min during the annealing procedure, respectively, while the corresponding Mn mappings are shown in Figs. 6(d), 6(f) and 6(h), respectively. The elemental mapping was acquired at RT by quenching the specimen right after certain annealing time, since the EDS detectors do not work properly at high temperature because of signal saturation induced by thermal radiation. The Mn distribution acquired at RT is still representative of the Mn distribution at elevated temperature since Mn atoms diffuse very slowly at RT.

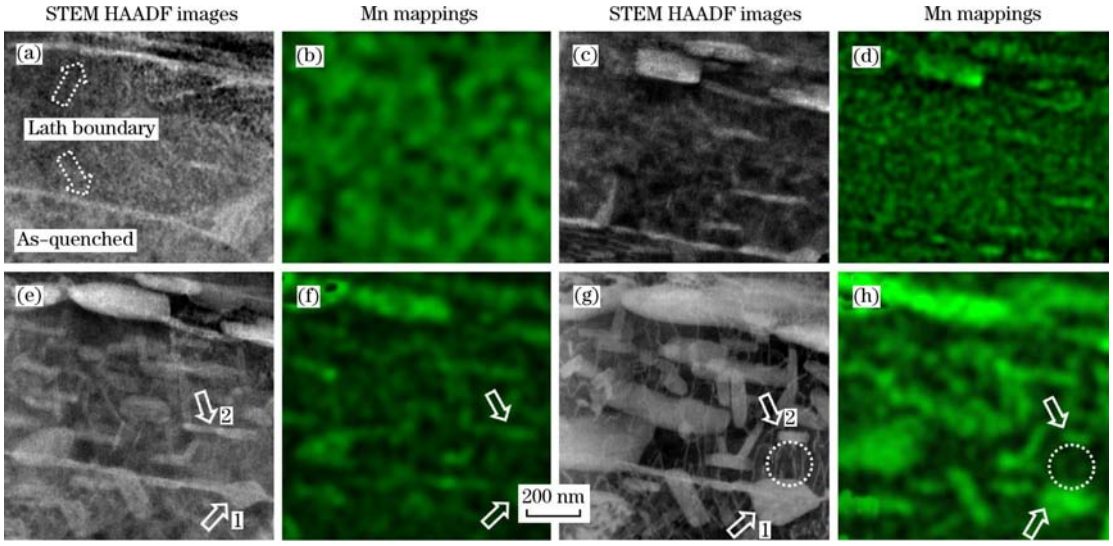

(a), (b) As-quenched specimen; (c), (d) Specimen annealed for 0 min; (e), (f) Specimen annealed for 12 min; (g), (h) Specimen annealed for 40 min.

Fig. 6. In-situ observation of microstructural evolution and corresponding Mn distribution in 5Mn steel during annealing at 500 ℃, with heating rate of 10 ℃/min.

The cementite formed and coarsened during heat treatment, since the original microstructure of as-quenched sample was full martensite lath without any cementite. At the early stage of the annealing procedure, most of cementite precipitates formed at lath boundaries, while some needle-shape cementite precipitates formed inside the laths. By comparing Mn mapping with the cementite morphology in scanning transmission electron microscopy high-angle annular dark field (STEM HAADF) images, there was Mn enrichment in both intragranular and intergranular cementite particles, indicating that the growth of cementite was controlled by Mn diffusion. Compared with intragranular cementite precipitates, the intergranular cementite precipitates had a larger size and grew preferentially along the lath boundaries. It was concluded that the diffusion rate of Mn atoms along lath boundaries was much higher than that within the laths. At the later stage of the annealing procedure, small cementite particles dissolved into large ones due to Ostwald ripening. It is noteworthy that the dislocations played an important role in Mn diffusion. As shown in Fig. 6(e,g), the large intergranular cementite particle and one small intragranular cementite particle are marked by "1" and "2", respectively, and connected by several dislocations. The small cementite particle "2" dissolved into the large particle "1" through dislocations during in-situ annealing. The corresponding Mn mapping as shown in Fig. 6(h) verified the significant Mn enrichment at the dislocations between two cementite particles, which was marked by the dotted circles in Fig. 6(g,h). The dislocation pipe mechanism of Mn diffusion can thus be confirmed during the growth of cementite.

4. Conclusion

Specimen of 5Mn steel was prepared by FIB milling and loaded on an advanced MEMS-based heating system, which allowed various in-situ TEM observations during heat treatments at different temperatures. The complete austenization of specimen was observed at the atomic scale at 800 ℃. When annealed at 650 ℃, the nucleation and growth of austenite were most likely to take place at matrix lath boundaries, while the morphology of reverted austenite laths after in-situ heating was quite similar to the typical morphology of 5Mn steel after ex-situ intercritical annealing. When annealed at 500 ℃, the coarsening of cementite was controlled by Mn diffusion. The Mn diffusion at lath boundaries was faster than that within the matrix, resulting in the growth

of intergranular cementite faster than intragranular cementite. The dislocations also served as an approach of Mn diffusion during the growth of cementite. The capability to observe the microstructural evolution of steel in real time at high spatial resolution provides insight into material transformation processes and mechanisms of complicated phase transition in steels.

Acknowledgment

This research was funded by National Basic Research Program of China (2010CB630800, 2015CB921700), National Natural Science Foundation of China (51671112, 51471096, 51390471, 11374174), National Key Research and Development Program (2016YFB0700402), National Key Scientific Instruments and Equipment Development Project (2013YQ120353) and Tsinghua University (20141081200). The authors acknowledge Dr. Qiang Xu at DENS Solution, Professor Henny W. Zandbergen at Delft University of Technology, Professor Jing Zhu, Professor Yuefeng Zhu, Mr. Yun-jie Yan and Mr. Feng Wang at Tsinghua University, Dr. Wen-quan Cao at Central Iron and Steel Research Institute, Prof. Yong Wang, Prof. Chuan-hong Jin and Ms. Ying Jiang at Zhejiang University, Dr. Hui Wang and Dr. Youxing Yu at Beihang University for the helpful assistance to the experiments of this work. The authors are also grateful to Dr. Tao Pan and CISRI-TCS United Open Laboratory for the permission to use Thermo-Calc software. This work made use of the resources of National Center for Electron Microscopy in Beijing, Center of Electron Microscope in Zhejiang University and Kavli Institute of Nanoscience in Delft University of Technology.

References

[1] W. Q. Cao, C. Wang, J. Shi, M. Q. Wang, W. J. Hui, H. Dong, Mater. Sci. Eng. A 528 (2011) 6661-6666.
[2] J. Shi, X. J. Sun, M. Q. Wang, W. J. Hui, H. Dong, W. Q. Cao, Scripta Mater. 63 (2010) 815-818.
[3] E. De Moor, D. K. Matlock, J. G. Speer, M. J. Merwin, Scripta Mater. 64 (2011) 185-188.
[4] S. Lee, S. J. Lee, B. C. De Cooman, Scripta Mater. 65 (2011) 225-228.
[5] C. Wang, J. Shi, C. Y. Wang, W. J. Hui, M. Q. Wang, H. Dong, W. Q. Cao, ISIJ Int. 51 (2011) 651-656.
[6] H. Luo, J. Shi, C. Wang, W. Cao, X. Sun, H. Dong, Acta Mater. 59 (2011) 4002-4014.
[7] R. Wei, M. Enomoto, R. Hadian, H. Zurob, G. Purdy, Acta Mater. 61 (2013) 697-707.
[8] X. N. Luo, X. Y. Zhong, H. W. Luo, H. H. Zhou, C. Y. Wang, J. Shi, J. Iron Steel Res. Int. 22 (2015) 1015-1019.
[9] B. A. Lindsley, A. R. Marder, Acta Mater. 46 (1998) 341-351.
[10] W. J. Nam, C. M. Bae, Scripta Mater. 41 (1999) 313-318.
[11] X. Q. Zhao, T. Pan, Q. F. Wang, H. Su, C. F. Yang, Q. X. Yang, J. Iron Steel Res. Int. 18 (2011) No. 5, 47-51.
[12] Y. Xia, X. N. Luo, X. Y. Zhong, H. H. Zhou, C. Y. Wang, J. Shi, J. Iron Steel Res. Int. 23 (2016) 442-446.
[13] J. Lin, X. N. Luo, X. Y. Zhong, H. H. Zhou, C. Y. Wang, J. Shi, H. Dong, J. Iron Steel Res. Int. 23 (2016) 1277-1280.
[14] H. P. Longworth, C. V. Thompson, J. Appl. Phys. 69 (1991) 3929-3940.
[15] P. Zheng, M. O. Ruault, M. F. Denanot, B. Descouts, P. Krauz, J. Appl. Phys. 69 (1991) 197-202.
[16] M. Legros, G. Dehm, R. M. Keller-Flaig, E. Arzt, K. J. Hemker, S. Suresh, Mater. Sci. Eng. A 463 (2001) 309-310.
[17] F. Radulescu, J. M. McCarthy, E. Stach, Mater. Res. Soc. Symp. Proc. 589 (2000) 179-184.
[18] M. A. Van Huis, N. P. Young, G. Pandraud, J. F. Creemer, D. Vanmaekelbergh, A. I. Kirkland, H. W. Zandbergen, Adv. Mater. 21 (2009) 4992-4995.
[19] A. Figuerola, M. Van Huis, M. Zanella, A. Genovese, S. Marras, A. Falqui, H. W. Zandbergen, R. Cingolani, L. Manna, Nano Lett. 10 (2010) 3028-3036.
[20] M. Duchamp, Q. Xu, R. E. Dunin-Borkowski, Microsc. Microanal. 20 (2014) 1-8.
[21] L. A. Giannuzzi, J. L. Drown, S. R. Brown, R. B. Irwin, F. A. Stevie, Mater. Res. Soc. Symp. Proc. 480 (1997) 19-27.
[22] Q. Jeangros, A. Faes, J. B. Wagner, T. W. Hansen, J. Van Herle, A. Hessler-Wyser, R. E. Dunin-Borkowski, Acta Mater. 58 (2010) 4578-4589.
[23] H. Wang, S. G. Xiao, Q. Xu, T. Zhang, H. W. Zandbergen, Mater. Sci. Forum 850 (2016) 722-727.